Title
Detector concept for OPET - A combined PET and optical Imaging system

Journal
IEEE Transactions on Nuclear Science, 51(3)

ISSN
0018-9499

Authors
Prout, D L
Silverman, R W
Chatziioannou, A

Publication Date
2004-06-01

Peer reviewed

Detector Concept for OPET—A Combined PET and Optical Imaging System

D. L. Prout, *Member, IEEE*, R. W. Silverman, *Senior Member, IEEE*, and A. Chatziioannou, *Member, IEEE*

***Abstract*—The design of an imaging system capable of detecting both high-energy γ-rays and optical wavelength photons is underway at the UCLA Crump Institute for Molecular Imaging. This system, which we call optical PET (OPET), will be capable of noninvasively and repeatedly imaging small animal models *in vivo* for the presence of PET and optical signals. In this study, we describe the physical principles behind the operation of the OPET imaging system and discuss the design concept for one of the detector modules. Additionally, we demonstrate the operation of an initial prototype detector module for simultaneous detection and imaging of annihilation radiation and single optical photons emanating from separate sources. These results indicate that the construction of an imaging system based on this detector technology is feasible.**

***Index Terms*—Bioluminescence, microPET, positron emission tomography (PET), small animal imaging.**

I. Introduction

OPTICAL imaging is an essential tool at the disposal of biological researchers. Due to the poor penetration of visible light photons in mammalian tissues [1], optical imaging techniques have been mostly limited to surface applications in humans. Still though, these techniques continue to have tremendous impact in cellular and molecular biology research and are now finding significant applications in *in vivo* small animal imaging [2]. Translation of these scientific advances to human applications is facilitated with the development of dual molecular imaging probes, presenting both optical and PET signals [3]. OPET is a device designed to facilitate the translation of biological research and knowledge between the optical and PET realms by imaging small animal models and capable of detecting and simultaneously imaging both PET and optical signals. One could for example, image radiolabeled luciferin, to evaluate the temporal and spatial distribution of the substrate availability in tissue, especially in situations where the blood flow is impaired such as in infarct models, or tumors with poor vascularity [4].

In this work, first we describe the relevant physical principles of the two imaging devices that we are combining into a single system in OPET. Next, by considering the nature of the signals in optical and PET measurements, we show how a single detector may be designed and constructed to record both signals. Finally, we outline an imaging system concept for the OPET tomograph and then present results from tests of a prototype OPET detector module.

Manuscript received November 15, 2003; revised March 3, 2004. This work was supported in part by the U.S. Department of Energy under Contract DE-FC03-02ER63420 and in part by the National Institutes of Health under Grant R24 CA92865 and EB001458.

The authors are with the Crump Institute for Molecular Imaging at the Geffen School of Medicine, University of California at Los Angeles (UCLA), Los Angeles, CA 90095 USA (e-mail: dprout@mednet.ucla.edu; bsilverman@mednet.ucla.edu; archatziioann@mednet.ucla.edu).

Digital Object Identifier 10.1109/TNS.2004.829736

II. Bioluminescence (Optical) Setup

A typical bioluminescence study involves injection of a substrate (luciferin) into a subject containing genetically engineered cells that produce the enzyme luciferase. Photons in the range from 510 to 700 nm are emitted in the reaction of luciferin, oxygen, and ATP catalyzed by luciferase. For the animal of interest, the mouse, the large attenuation of photons with wavelengths below 600 nm, even for cells implanted subcutaneously, results in an emitted spectrum peaked at around 610 nm [5].

Because of the significant light attenuation, cooled charged coupled devices (CCD) are typically required to detect the limited number of photons emitted from the surface of the mouse. For our study, we used the commercial IVIS® System (Xenogen Inc. Alameda, CA) as a reference. This system consists of a cooled CCD camera mounted in a light tight black box. Photons from the mouse are focused or "coupled" to the CCD with a high quality $f/1$ lens. The overall number of photons is "counted" through charge integration on the CCD, providing a 2-D image of the emitted light from the mouse. This image is superimposed on a conventional grayscale photograph of the reflected light to provide anatomical orientation [2]. Exposure times range from a few seconds to a few minutes for typical studies. For this setup, the arrival time of each photon in the CCD is not available.

While the spatial resolution of the IVIS® System is excellent (on the order of micrometers), the resolution requirements on the instrumentation for *in vivo* mouse studies is much lower—on the order of a few millimeters bioluminescence. That is because unabsorbed optical wavelength photons are highly scattered in mouse tissues and therefore greatly reduce the intrinsic spatial resolution of the optical signal. For example, a point source of light embedded in 4 mm of tissue will produce a broad distribution on the surface with a FWHM of 5–6 mm [5].

III. Small Animal PET

The microPET scanner design and performance is described in detail elsewhere [6], [7]. Relevant to this article are the detector modules that are required to determine both the position and arrival time of annihilation photons.

A detector suitable for use in small animal PET imaging systems contains a scintillation crystal array for conversion of the annihilation γ-rays to low energy visible light photons, and a multichannel or position sensitive photodetector used to detect

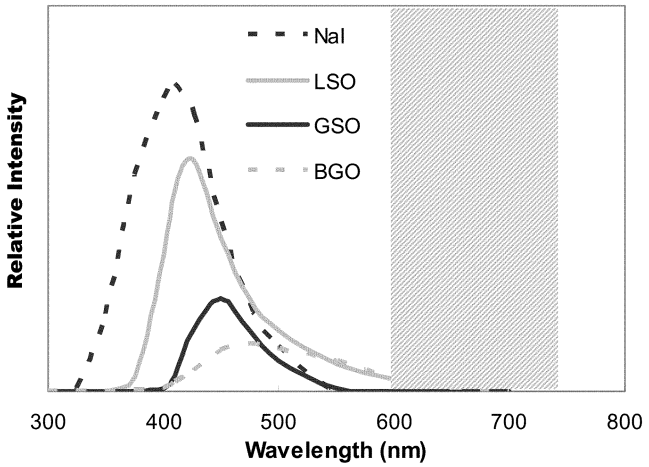

Fig. 1. The curves represent spectra of emitted light from various scintillation crystals. The wavelength of scintillation light is in the range 350–550 nm and generally shorter wavelength than the light generated through bioluminescence and propagated through tissue. The shaded area indicates the wavelength range encountered through bioluminescence light that has propagated through a minimal amount of tissue.

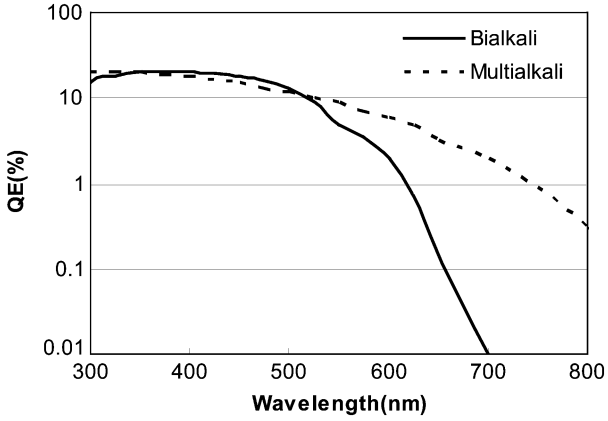

Fig. 2. Comparison of quantum efficiency for standard bialkali photocathode used in the MC-PMT with that of a multi-alkali photocathode.

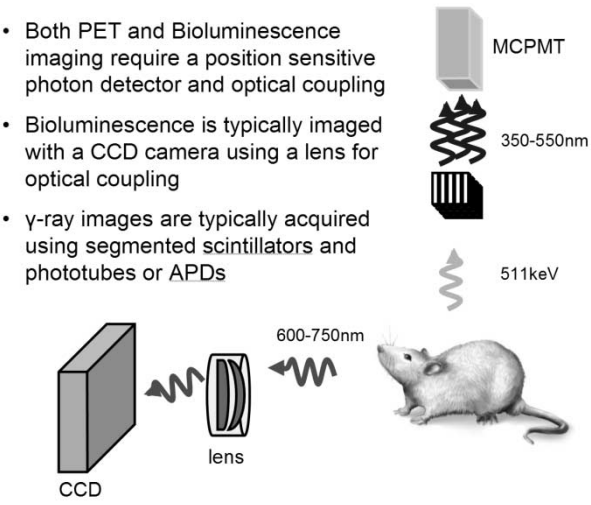

Fig. 3. Schematic that illustrates the basic principles and components of detectors for optical and PET imaging systems.

them. Both solid state and vacuum tube technologies are suitable as photodetectors [8], [9]. In this case, the PET detector scintillators are crystals of dimensions $2 \times 2 \times 10$ mm, wrapped with a reflective material and packed into an array of 64 optically isolated crystals. The spectrum of light generated when a γ-ray interacts with one of these crystals is shown in Fig. 1 for a number of common scintillator materials [10]. The photons correspond to wavelengths in the blue green region of the spectrum (350–550 nm) in contrast to photons emitted from the animals in the case of bioluminescence (600–750 nm), which is illustrated in Fig. 1.

Avalanche photodiodes (APDs) arrays and multichannel photomultiplier tubes (MC-PMTs) are used as photodetectors for PET scanners since they can provide both positional and temporal information. Conventional MC-PMTs employ bialkali photocathodes to match the wavelengths of photons generated by the scintillation crystals. The typical quantum efficiency (QE) of the MC-PMTs is shown as the solid line in Fig. 2. The QE at scintillation wavelengths is around 20%. Typical MC-PMTs now used for PET have a square face, an active area of 22×22 mm and consist of multiple separate channels. Spatial resolutions better than 1 mm have been obtained with such PET modules [11].

IV. Combined System

In Fig. 3, we present a schematic demonstrating the two separate schemes for detecting bioluminescence photons and annihilation γ-rays for PET. The type of photodetector used for either optical or for PET imaging, is dictated by the different characteristics of the photons that need to be detected by the two different imaging modalities. PET requires a fast (nanosecond) photon counting detector, while imaging of optical photons is typically performed with slow photon integrating CCD cameras that have high quantum efficiency throughout the optical spectrum (>60%).

In order to combine the imaging of both signals into a single detector we require that the detector be sensitive to both the blue and red wavelength photons. In addition, the detector must be sensitive enough to register the single photons generated from biolumenescence and have a large enough dynamic range to handle the large bursts of photons produced in γ-ray interactions in the scintiallation crystal.

With these considerations, we designed a single detector module to be used in the OPET system, which will allow the measurement of the position of both γ-ray events and optical wavelength photons emanating from the surface of a mouse. We will eliminate the CCD and lens and use the scintillation array with an open end and photomultiplier tube for detection of both γ-rays and optical photons.

Example geometry for a single ring OPET system is shown in Fig. 4. The detector module geometry can be seen as well and will consist of a 64-channel photomultiplier tube. Coupled to the tube is a $2 \times 2 \times 10$ mm^3 array of crystals that serve as both scintillators for the interaction of the γ-rays and as *light guides* for the optical wavelength photons. To allow the red wavelength

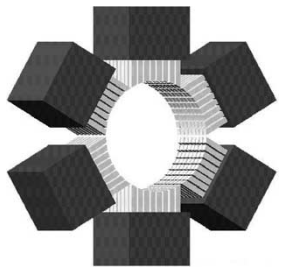

Fig. 4. Illustration of a single OPET detector ring showing the individual detector modules. Each module consists of a multichannel photomultiplier coupled to a scintillator array in which each crystal is optically isolated from the next.

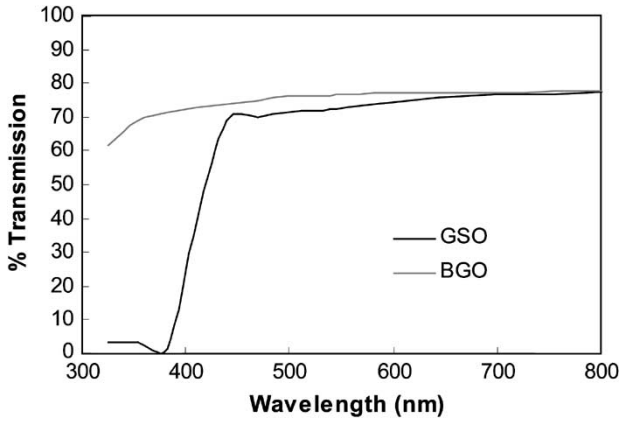

Fig. 5. Wavelength dependence of optical photon transmission through 1 cm thick scintillator crystal.

photons from the surface of the mouse into the crystal and onwards to the PMT, the crystal will have to be optically open on both ends.

The detector will function as a PET module [6] in the presence of annihilation γ-rays. For optical imaging, the surface of the mouse will be placed directly against the crystals and the location of the light will be determined by crystal identification.

V. Preliminary Tests

A. Detector Requirements

In order for the detector to function as both optical and γ-ray detector, it must satisfy a number of requirements: (i) The scintillator array must be capable of transmitting long wavelength photons from the animal to the photodetector; (ii) the detector must be capable of detecting and imaging individual light photons; (iii) the photodetector must be sufficiently sensitive to these photons to allow experiments comparable to those performed with CCD/lens based systems; and (iv) the spatial resolution of this detector needs to be on the order of 2 mm, to avoid degradation of optical signal spatial resolution for most of the mouse body.

B. Detector Transmission Tests

In Fig. 5, we plot the transmission of light through 1 cm thick GSO and BGO scintillators as a function of wavelength. These data were obtained using a Beckman DU-65 spectrophotometer (Beckman Inc., Fullerton, CA). The crystal was placed within the sample compartment in the light path between a variable wavelength, monochromatic source and the photo detector. The transmission for the wavelengths of interest for optical imaging (600–750 nm) is about 70%–75% and is sufficient for this application.

C. Imaging With a Multi-Alkali MC-PMT

In order to demonstrate that single photons and γ-rays can be simultaneously imaged using the proposed detector module, we obtained an 8×8 GSO scintillation array from Hitachi (Marubeni Chemicals Inc., White Plains, NY) and mounted it on an MC-PMT. A similar crystal array made from LSO was also tested, but it presented high afterglow that rendered it unusable for the application. Large afterglow effects in LSO excited by γ-rays has also been reported by others [12]. Each of the GSO crystals had a 2×2 mm cross-section and was 15 mm long. These crystals were optically isolated from each other by a thin grid of reflector forming a 64 element square array. The ends of the crystal array were left open with one end attached by optical grease to the MC-PMT. We obtained a prototype H7546 MC-PMT from Hamamatsu (Hamamatsu Photonics, Bridgewater, NJ) with an extended red sensitive multi-alkali photocathode in order to boost the efficiency of the tube to red wavelength photons. As seen from the quantum efficiencies plotted in Fig. 2, the use of a tube with such a photocathode could increase the sensitivity to these photons (600–750 nm) by a factor of 4–5 above bialkali MC-PMTs. The prototype MC-PMT has an active area that matched the dimensions of the GSO crystal array.

The MC-PMT and GSO array were placed in a light tight black box along with a red wavelength light emitting diode (LED). An "optical" mask was placed on top of the GSO array in order to form a distinctive light photon pattern entering the crystal array. The mask was a 2.5×2.5 cm black photographic paper with seven 2×2 mm holes cut in it and is displayed in Fig. 6(a). A 5 μCi positron emitting ^{22}Na source was placed $\sim$2 mm from the crystal array and the LED was flashed while both γ-ray and optical data were acquired. The data acquisition and event separation was performed with a special readout circuit described elsewhere [13]. In principle, single photon events were acquired between occurrences of the large pulses generated by the γ-ray events.

Shown in Fig. 6 are the images produced by the optical events (b) and the γ-ray events (c). The pattern of the optical mask providing the visible light input is evident in Fig. 6(b), however, one of the holes is missing and in general the intensity in the upper edge of the image is significantly lower than that of the bottom half of the image. Flood measurements performed by flashing the LED with no mask revealed that the sensitivity of the photocathode to red wavelength photons was nonuniform and was especially weak in the upper portion of the MC-PMT. The pattern for the γ-ray events shown in Fig. 6(c) is typical of "flood" histograms routinely obtained from such detectors [14]. The response of the photocathode of this early prototype PMT to the blue-wavelength photons generated by the γ-ray interaction in the crystal is apparently more uniform than the phototube's response to red wavelength photons as we did

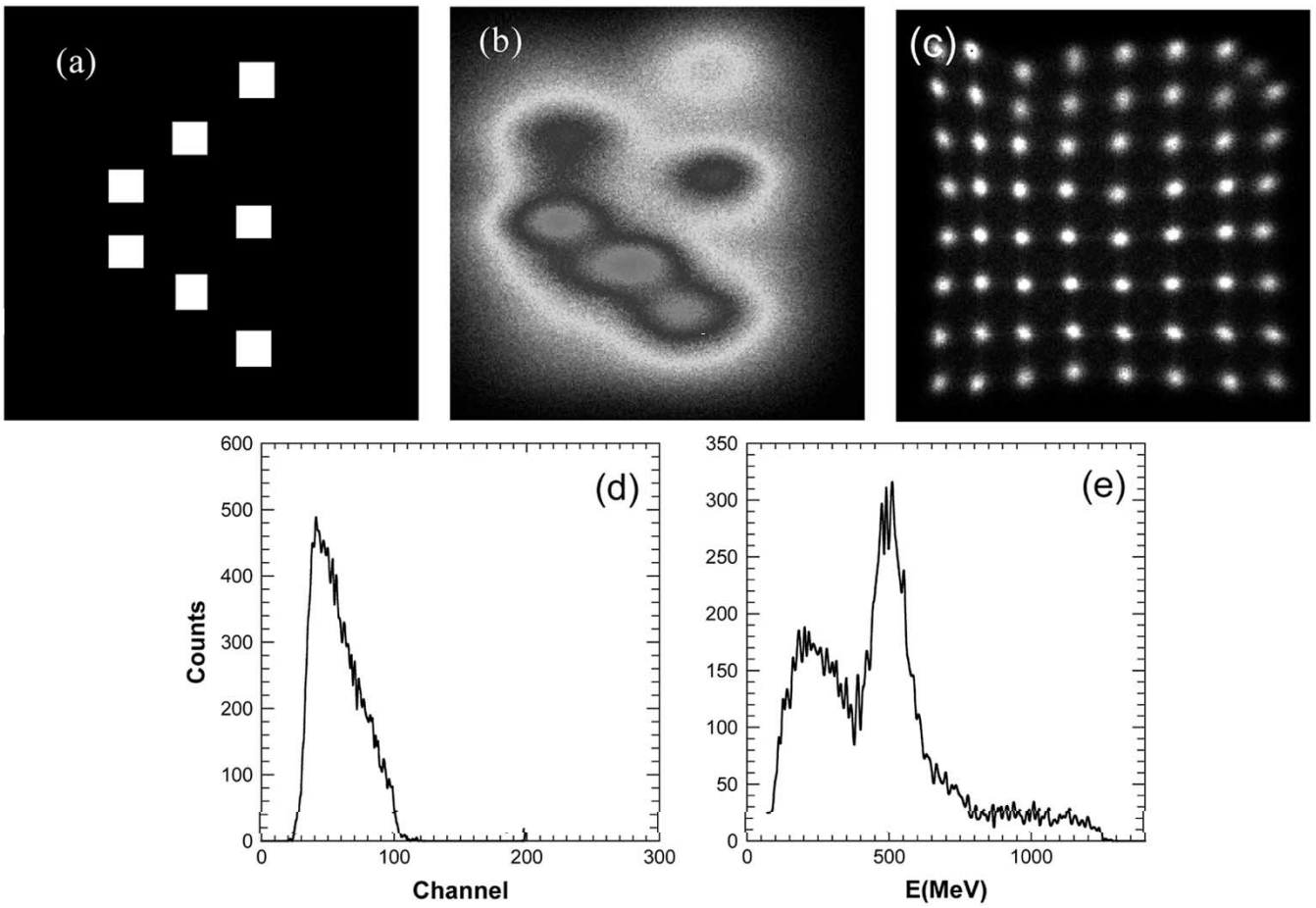

Fig. 6. (a) An optical mask was placed on a GSO array coupled to a multalkali MC-PMT. (b) The optical image was obtained from a red LED placed nearby. (c) At the same time, a "flood" histogram was acquired from γ-rays emitted by a ^{22}Na source placed near the array. (d) The single photoelectron spectrum (SPE) from one of the bright areas of the optical image is shown. (e) An energy spectrum due to γ-ray interactions in one of the crystals is shown.

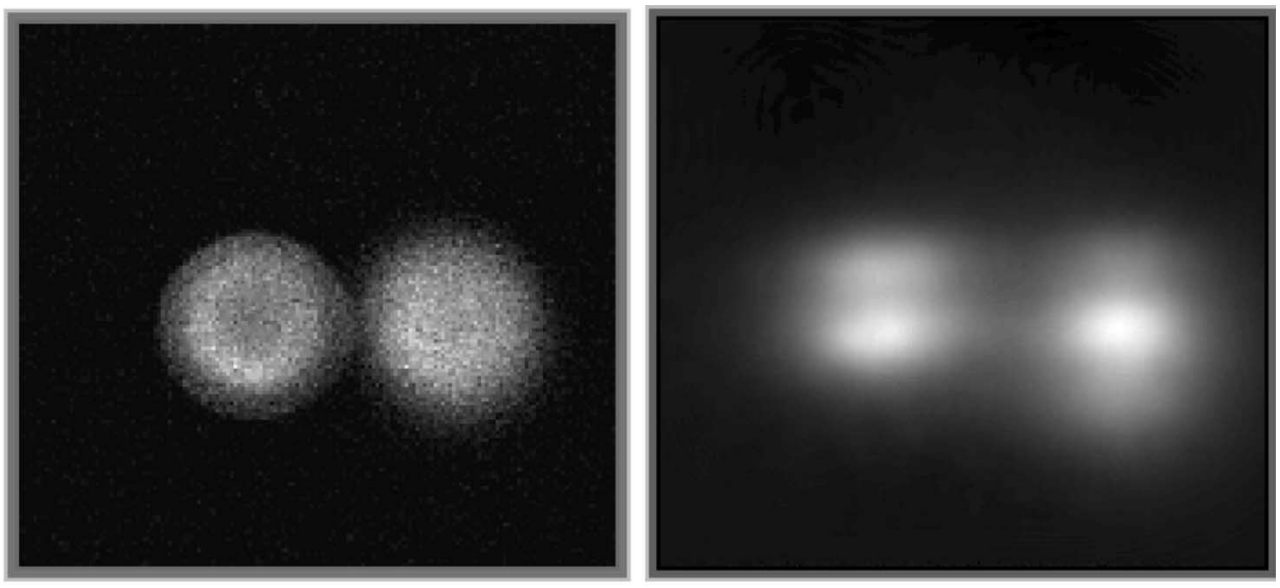

Fig. 7. Sensitivity test of the OPET module was performed with two calibrated red wavelength LEDs. In the left panel is the image produced in the Xenogen IVIS® System. On the right is the same light source set in direct contact with the OPET detector module. In both images a background image has been subtracted. The count rates in the bright area of the images were used to compare sensitivities and the results are displayed in Table I.

not observe a marked difference in sensitivity as a function of position in the γ-ray image. We expect future "production quality" MC-PMTs to exhibit improved uniformity in the red wavelength response.

TABLE I
RESULTS FOR INITIAL SENSITIVITY TEST OF THE PROTOTYPE OPET DETECTOR MODULE COMPARED TO THE IVIS® SYSTEM. THE COUNT RATES REPRESENT THE NUMBER OF COUNTS IN THE BRIGHT AREAS OF FIG. 7 AFTER BACKGROUND SUBTRACTION. THE FIRST ROW INDICATES THE PHOTON FLUX OF THE TWO SOURCES. THE IVIS® DATA WERE TAKEN WITH A 10 cm FOV. THIS CORRESPONDS TO A DISTANCE OF ABOUT 25 cm TO THE F/1 LENS OF THE CCD CAMERA

	Source 1	*Source 2*
Flux (ph/s)	$5.3\text{x}10^5$	$6.2\text{x}10^5$
IVIS® (cps)	1670	1920
OPET (cps)	1240	1660

In Figs. 6(d) and (e), we display spectra corresponding to one of the bright spots in Figs. 6(b) and (c). The events in the region around the brightest spot in Fig. 6(b) were histogrammed with respect to the amplitude of the event, and resulted in the typical single photon spectrum in Fig. 6(d). For Fig. 6(e), one of the crystals near the middle of the image was selected and these γ-ray events were histogrammed. The photopeak due to the 511 keV annihilation γ-rays is evident in this figure.

These images and spectra demonstrate simultaneous imaging of both γ-rays and red-wavelength photons. The experiments were performed at count rates typical for PET ($\sim$4000 cps for singles). Further studies will be necessary to ascertain the degree to which the two signals interfere with each other, and especially the effect of afterglow of the scintillator on the optical image.

D. Sensitivity Tests

We measured the sensitivity of the detector module described in the last section with a low-level light source used for quality control of the IVIS® CCD System. The flux of photons from two red-wavelength LEDs (635 ± 45 nm) provided with the light source was measured with the Xenogen IVIS® System. Each LED was covered with material, which created a diffuse spot of approximately 1 cm diameter while the two sources were separated by 1 cm center-to-center. These measurements revealed a photon flux of 5.3×10^5 photons/s (ph/s) into 4π steradians for one source and 6.2×10^5 ph/s for the other. The light source was placed on the GSO crystal array and a 5-min acquisition was performed in the presence of a ^{22}Na source which provided an annihilation γ-ray count rate of $\sim$5000 cps. In Fig. 7, we show the image obtained from both the IVIS® measurement and the measurement with the prototype detector. In both cases, background measurements were performed and the results subtracted. The presence of two sources is evident in both images. In the right image, the variation in the bright areas is apparently associated with the dynode structure of the MC-PMT. We have integrated the counts in the bright areas of both figures and the results are displayed in Table I. While these results are preliminary, the observed count rates for optical events indicate that this prototype OPET detector module should have comparable sensitivity to the IVIS® System. We expect the OPET detector sensitivity to increase with improvements in the readout electronics that will allow more accurate adjustment of the low level threshold. Further studies of this detector module are underway.

VI. SUMMARY

We presented a conceptual design for a detector module to be used in the OPET imaging system. We demonstrated that such a detector can be nearly as sensitive to bioluminescent light as state-of-the-art lens coupled CCD-based systems. Simultaneous imaging of optical wavelength photons and γ-rays was also shown for a red sensitive MC-PMT.

ACKNOWLEDGMENT

The authors wish to thank Xenogen for helpful discussions, P. Chow for work on the drawings of OPET and Marubeni (Hitachi) Specialty Chemicals, Photon Imaging, and R. Slates for use of the GSO crystals. They also thank Hamamatsu Corporation for providing the prototype MC-PMT.

REFERENCES

[1] W. F. Cheong, S. A. Prahl, and A. J. Welch, "A review of the optical-properties of biological tissues," *IEEE J. Quantum Electron.*, vol. 26, pp. 2166–2185, 1990.
[2] C. H. Contag, D. Jenkins, F. R. Contag, and R. S. Negrin, "Use of reporter genes for optical measurements of neoplastic disease *in vivo*," *Neoplasia*, vol. 2, pp. 41–52, 2000.
[3] P. Ray, A. M. Wu, and S. S. Gambhir, "Optical bioluminescence and positron emission tomography imaging of a novel fusion reporter gene in tumor xenografts of living mice," *Cancer Res.*, vol. 63, pp. 1160–1165, 2003.
[4] F. Berger, R. Paulmurugan, and S. S. Gambhir, "Uptake kinetics and biodistribution of ^{14}C D-luciferin, a radiolabeled substrate for the firefly luciferase catalyzed bioluminescent reaction," *J. Nucl. Med.*, vol. 44, pp. 317P–317P, 2003.
[5] B. W. Rice, M. D. Cable, and M. B. Nelson, "*In vivo* imaging of light-emitting probes," *J. Biomed. Opt.*, vol. 6, pp. 432–440, 2001.
[6] S. R. Cherry, Y. Shao, M. P. Tornai, S. Siegel, A. R. Ricci, and M. E. Phelps, "Collection of scintillation light from small BGO crystals," *IEEE Trans. Nucl. Sci.*, vol. 42, pp. 1058–1063, 1995.
[7] A. F. Chatziioannou, S. R. Cherry, Y. Shao, R. W. Silverman, K. Meadors, T. H. Farquhar, M. Pedarsani, and M. E. Phelps, "Performance evaluation of microPET: A high-resolution lutetium oxyorthosilicate PET scanner for animal imaging," *J. Nucl. Med.*, vol. 40, pp. 1164–1175, 1999.
[8] C. J. Marriott, J. E. Cadorette, R. Lecomte, V. Scasnar, J. Rousseau, and J. E. van Lier, "High-resolution PET imaging and quantitation of pharmaceutical biodistributions in a small animal using avalanche photodiode detectors," *J. Nucl. Med.*, vol. 35, pp. 1390–1396, 1994.
[9] M. E. Casey and R. Nutt, "A multicrystal two dimensional BGO detector system for positron emission tomography," *IEEE Trans. Nucl. Sci.*, vol. NS-33, pp. 460–463, 1986.
[10] C. L. Melcher and J. S. Schweitzer, "Cerium-doped lutetium oxyorthosilicate: A fast, efficient new scintillator," *IEEE Trans. Nucl. Sci.*, vol. 39, pp. 502–5, 1992.
[11] R. S. Miyaoka, S. G. Kohlmyer, and T. K. Lewellen, "Performance characteristics of micro crystal element (MiCE) detectors," *IEEE Trans. Nucl. Sci.*, vol. 48, pp. 1403–1407, 2001.
[12] J. G. Rogers and C. J. Batty, "Afterglow in LSO and its possible effect on energy resolution," *IEEE Trans. Nucl. Sci.*, vol. 47, pp. 438–445, 2000.
[13] D. L. Prout, R. W. Silverman, and A. Chatziioannou, "Readout of the optical OPET detector," presented at the *Proc. 2003 IEEE Nuclear Science Symp./Medical Imaging Conf.*, Portland, OR, 2003.
[14] A. Chatziioannou, Y. C. Tai, N. Doshi, and S. R. Cherry, "Detector development for microPET II: A 1 mu l resolution PET scanner for small animal imaging," *Phys. Med. Biol.*, vol. 46, pp. 2899–2910, 2001.